INSTITUTE OF PHYSICS PUBLISHING SMART MATERIALS AND STRUCTURES
Smart Mater. Struct. **15** (2006) 737–748 doi:10.1088/0964-1726/15/3/009

# A carbon nanotube strain sensor for structural health monitoring

**Inpil Kang**[1], **Mark J Schulz**[1,3], **Jay H Kim**[1], **Vesselin Shanov**[2] **and Donglu Shi**[2]

[1] Department of Mechanical Engineering, Smart Materials Nanotechnology Laboratory, University of Cincinnati, Cincinnati, OH 45221-0072, USA
[2] Department of Chemical and Materials Engineering, University of Cincinnati, Cincinnati, OH 45221-0012, USA

E-mail: Mark.J.Schulz@uc.edu

Received 7 February 2005, in final form 16 February 2006
Published 25 April 2006
Online at stacks.iop.org/SMS/15/737

**Abstract**
A carbon nanotube polymer material was used to form a piezoresistive strain sensor for structural health monitoring applications. The polymer improves the interfacial bonding between the nanotubes. Previous single walled carbon nanotube buckypaper sensors produced distorted strain measurements because the van der Waals attraction force allowed axial slipping of the smooth surfaces of the nanotubes. The polymer sensor uses larger multi-walled carbon nanotubes which improve the strain transfer, repeatability and linearity of the sensor. An electrical model of the nanotube strain sensor was derived based on electrochemical impedance spectroscopy and strain testing. The model is useful for designing nanotube sensor systems. A biomimetic artificial neuron was developed by extending the length of the sensor. The neuron is a long continuous strain sensor that has a low cost, is simple to install and is lightweight. The neuron has a low bandwidth and adequate strain sensitivity. The neuron sensor is particularly useful for detecting large strains and cracking, and can reduce the number of channels of data acquisition needed for the health monitoring of large structures.

(Some figures in this article are in colour only in the electronic version)

## 1. Introduction

Smart materials developed using nanotechnology have the potential to improve the way we generate and measure motion in devices from the nanoscale to the macroscale in size. Among several possible smart nanoscale materials, carbon nanotubes (CNTs) [1–69] have aroused great interest amongst researchers because of their remarkable mechanical, electrochemical, piezoresistive and other physical properties. It is predicted that integrating CNT materials into polymers will open up a whole range of smart structure applications [2, 3]. CNTs are currently of interest in the building of advanced sensors [4–7] and actuators [8–10] for applications that require high force and stiffness and self-sensing of motion. CNTs are the strongest material possible, and are super-elastic and can be bent to large angles without breaking. Structural and electrical characteristics of CNTs include a large surface area, piezoresistivity and electrochemical properties that make them a promising smart sensor material. The electronic properties of nanotubes are interestingly a strong function of their atomic structure. Furthermore, mechanical deformation or chemical functionalization of the surface can induce changes in the conductance [11] of a nanotube. Their small size allows CNTs to be used as extremely small sensors that are sensitive to the chemical and mechanical environments of the nanotubes.

These great properties represent a potential for developing actuators with high stress, high strain and low operating voltage and for developing multifunctional sensory materials. In particular, the idea of using the piezoresistivity of CNTs (change in resistance with strain) and the possibility of making a long fiber to be used as a neuron may produce a useful new

[3] http://www.min.uc.edu/∼mschulz/smartlab/smartlab.html

strain sensor. Such a sensor could measure large strain and form a grid over a large area of a structure for structural health monitoring (SHM) applications. Also, unlike other smart materials, CNTs are potentially simultaneously structural, functional and smart materials because of their load carrying capability, high thermal and electrical conductivity and sensing properties. A polymer nanocomposite material containing about 1 per cent of single walled carbon nanotubes (SWNTs) can become a self-sensing structure if an electrode is applied to the composite surfaces. Another approach is to form thin films of the CNT polymer on the surface of a structure to monitor the structure for damage. Building smart structural materials that can actuate and self-sense by casting CNTs in a polymer material is a new approach to the design of smart structures.

Because of the small size of the sensor that is made possible by the application of nanotube smart materials, some researchers have studied the strain sensing properties of CNTs using Raman spectroscopy at the nanoscale [12]. Raman spectroscopy [13–15] can also be used at the macroscale for indirect measurement of the resistance of a nanocomposite. However, Raman spectroscopy is too bulky to be used in a sensor mechanism. In another approach, Watkins *et al* [69] used lithography and aligned SWNTs to fabricate a SHM sensor based on strain measurement. This microelectromechanical system (MEMS) technique can measure small strain and it can also detect very small cracks. However, this sensor would require a large signal processor due to the arrays of sensors that would be needed to cover a large area for SHM. In general, mechanical and civil engineering applications have large areas to be monitored and a simple SHM system with a minimum number of data acquisition channels would be desirable.

At the other extreme, there are difficulties when using nanotubes at the macroscale. Buckypaper is a thin sheet (film) formed using a well-controlled dispersion of CNTs in a solvent and evaporating the solvent to form a porous network of SWNTs. At the macroscale, fragility and the transfer of strain to the nanotubes in the buckypaper have been blocked the development of a dynamic strain sensor for practical applications. Also, Raman spectroscopy is not a practical sensing technique in the field of SHM because of its cost and complexity. To overcome these limitations, a nanocomposite material needs to be developed to minimize slip between adjacent nanotubes and between nanotubes and the polymer, and to increase the strain transfer and strength of the material. Also, strain measurement using the sensor would ideally follow a simple strategy like a conventional strain gage.

Hence, in this paper a composite electrical resistance strain sensor based on SWNTs is developed to measure the strain of a structure at the macroscale. Moreover, a multi-walled carbon nanotube (MWNT) polymer composite was built and tested as a continuous strain sensor. The MWNT sensor has a lower electrical performance but a lower cost than the SWNT sensor. The material processing approach developed herein reduces the problems of the buckypaper strain sensor and produces a nanocomposite strain sensor that is rugged and practical. In addition, a long CNT strain sensor is used to form a continuous neuron sensor for SHM. This is a preliminary study to develop a neuron which can detect high strain and cracks using a biomimetic artificial neural system (ANS) made of a CNT composite. The sensors developed in this study may lead to a new material system with applications to structures for civil and mechanical systems.

## 2. Fabrication and characterization of a SWNT based strain sensor

### *2.1. Buckypaper fabrication*

The inability to synthesize long nanotubes has been a serious obstacle to the use of CNTs in engineering applications. Because of the small size of CNTs and their high surface area, fabricating functional macroscale materials has been a major challenge for applications such as high capacity energy storage, sensor materials and electrochemical actuators. Dispersion during composite processing is required to produce a suspension of independently separated nanotubes that can be manipulated into preferred orientations for large scale applications. The nanotube bundles must be separated into tiny bundles using mechanical, chemical or combined methods. Even with multiple approaches, the dispersion of nanotubes is very challenging and the process depends on the quality and surface morphology of the nanotubes [17–19]. In this paper, various conditions for sample preparation are tried, although in many cases the best performance for real applications is still to be achieved. Mechanical dispersion using ultrasound or shear force mixing is the main approach used here to fabricate the SWNT based sensor. A limitation of this approach is that energy from mechanical methods can fragment the nanotubes and reduce the aspect ratio and degrade the electrical properties [20]. Because high energy ultrasound and excess sonication time cause defects and serious damage to CNTs, low power bath sonication is used here to maintain long tubes, rather than tip sonication [21] that improves dispersion but breaks the nanotubes. The ultrasound cavitation generated by the sonicator is so energetic it can break or strip the outer graphite layers of CNTs and it can completely cut the tubes from tangled nanotube ropes [22].

In this paper, commercially obtained SWNTs [23] were dispersed in dimethyl formamide (DMF) solvent, 1.5 mg $ml^{-1}$, and put in a bath sonicator (Branson 1510) for 20 h. After the dispersion processing, the SWNT suspension solution was poured into P8 filter paper, or a Teflon casting mold, and dried in a vacuum oven at 60–70 °C for 12 h to slowly evaporate the solvent. Then the freestanding buckypaper film ($\sim$20 $\mu$m thick) was peeled off. This film is composed of highly entangled SWNT bundles held together by van der Waals forces. Sonicating the SWNT ropes in the solvent causes inevitable defects during the dispersion process. Thus, the CNT should be partially healed and purified through an annealing process. It has been reported that the annealing process not only recovers the wall defects, but also improves the electrical properties of the CNT [24]. The annealing heat treatment at high temperature improves the electrical properties of the CNT sheet by removing the residual solvents and contaminants and improving the crystallinity [25]. In [26, 27] it is reported the annealing affects the electrochemical properties of the SWNTs. The annealed SWNTs have super-capacitance due to a large specific area produced by the small and uniform distribution of pore diameters. In this study the buckypaper was annealed in a furnace at 320 °C in air. The electrical

conductivity of the buckypaper improved with the annealing process, but in most the cases the buckypaper used for the strain sensor did not require much electrical improvement.

### *2.2. Fabrication of SWNT/polymethyl methacrylate composite sensor*

Ideally, strain applied to the structure is transferred to the nanotubes in the sensor. However, the buckypaper sensor has some slippage among the nanotubes in bundles because there is only weak bonding due to the van der Waals interactions at the junction points of the nanotubes. This may hamper strain transfer through the whole sensor and degrade strain measurements. Thus, a SWNT based composite material was fabricated to improve strain transfer across the nanotube sensor by means of better interfacial bonding. Adding a polymer to pristine nanotubes improves interfacial adhesion between the phases and achieves a stronger bond between the polymer and nanotubes by forming a helical polymer conformation [28]. In the literature, the interfacial adhesion of the nanotubes was found to improve due to an order of magnitude increase in the interfacial shear strength of the polymer material [29]. Since the nanotube–matrix interface is a critical parameter for controlling the mechanical and electrical properties of CNT composites, it is studied on the basis of polymer reinforcing techniques [30–33]. However, the physics of intercalation of CNTs to the binding matrix has yet to be clarified, and controlling dispersion is still a challenge.

In this study, polymethyl methacrylate (PMMA) was used as a polymer binding material because it is simple to handle and to mix with SWNTs in a solvent (DMF). PMMA was added to a suspension of SWNTs in DMF and mixed using shear force with a Dremel drill at 70 °C for 4 h. After the dissolving and mixing process, the liquid was cast in a Teflon mold to form a sheet and it was initially cured in a vacuum oven at room temperature for 30 min to remove air. It was then fully cured in a low vacuum (16 inch Hg), at 120 °C for 12 h to evaporate the solvent and to anneal the SWNTs in the binding material. Finally, the SWNT/PMMA composite film (∼85 $\mu$m thick) was detached from the mold. Optimized dispersion and polymer processing are required to give uniform and homogeneous samples for tests. However, this is challenging to achieve due to small variations in the SWNTs and the polymer processing. Apparently small variations in multiple processing parameters can have a significant effect on the overall properties.

### *2.3. Electrical characterization and modeling of the sensor in an electrolyte*

Electrochemical impedance spectroscopy (EIS) testing was performed to characterize the electrical properties of the SWNT/PMMA sensor material and to help develop an electrical model of the material. EIS testing is a basic characterization method that analyzes the electrokinetics of the material in relation to the conduction and capacitance of the sensor [3]. The properties of the sensor strongly depend on the material processing because it is a nanocomposite. Therefore, the electrical properties of the sensor were studied using electrochemical impedance spectroscopy. It was then attempted to relate the electrical properties to the nanocomposite processing including the functionalization, dispersion and annealing of the nanotubes. EIS is a frequency response type analysis using a wet test cell based on electrochemistry. The EIS is usually measured by applying a small amplitude AC potential and a fixed DC potential to an electrochemical cell and measuring the current through the cell. A sinusoidal potential excitation is often applied. The response to this potential is an AC current signal, containing the excitation frequency and its harmonics. This current signal can be analyzed as a sum of sinusoidal functions [36]. The impedance varies with frequency and is often plotted in different ways to make it a spectroscopic technique [37]. The EIS cell consists of a working electrode, which is the SWNT or PMMA/SWNT composite sample, a Pt plate counter electrode, and a reference electrode which in this study was a saturated calomel electrode (SCE) in 3% NaCl electrolyte. This setup describes a potentiostat, which is an electronic device that controls the voltage difference between a working electrode and a reference electrode. Both electrodes are contained in the electrochemical cell. The potentiostat implements this control by injecting current into the cell through the auxiliary, or counter, electrode and the potentiostat measures the current flow between the working and auxiliary electrodes. The controlled variable in the potentiostat is the cell potential and the measured variable is the cell current.

For testing of the sensor material, 3 mm × 5 mm × ∼0.3 mm pieces of the SWNT/PMMA composite were fabricated. Buckypaper samples were also fabricated for comparison. The EIS measurements were performed using a Gamry potentiostat (model PCI4/750) coupled with EIS software (Gamry, EIS300). Figure 1 shows the complex-plane impedance plot with 0.4 V bias voltage and the cyclic voltammetry (CV) [36, 38] behavior of samples at a scan rate of 100 mV $s^{-1}$ in the electrolyte. The Nyquist diagrams in figures 1(a), (c) show improved conductivity after annealing. The CV diagrams in figures 1(b) and (d) show an expansion of area which means the capacitance is increasing after annealing [26].

The EIS test shows the complex-plane impedance plot and it also shows the electrical parameters and allows equivalent circuit modeling of the sensor based on the frequency response. Electrical modeling of CNTs can be a combination of resistance, inductance and capacitance (R, L and C, respectively) [39–44] elements. The electrical properties of buckypaper and the composite strain sensor can be modeled as Randles' circuit which is an equivalent parallel RC circuit representing each component at the interface and in the solution during an electrochemical reaction. Above 1 Hz, the circuit parameters correspond to the physical system of a double layer capacitor ($C_d$), polarization resistance ($R_p$) and Warburg coefficient ($W$), as shown in figures 2(a) and (b) [36]. The PMMA polymer composite sensor can be modeled using the Warburg impedance due to a combination of kinetic and diffusion processes, but these effects are neglected in the circuit model here due to their minor effect for strain sensing. Table 1 shows the estimated electrical parameters of the samples that were determined using the EIS test. The parameters are extracted from the EIS data using the curve fitting algorithm within the EIS software. We can predict the performance of the sensor and study the effect of the annealing process using these parameters.

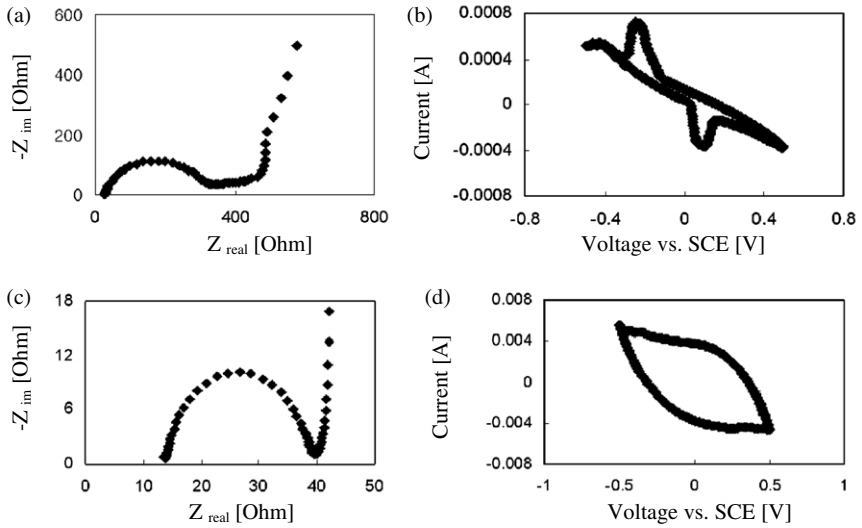


**Figure 1.** Electrical impedance spectroscopy (EIS) test of buckypaper in 3% NaCl electrolyte: (a) Nyquist diagram for buckypaper that is not annealed; (b) CV diagram of buckypaper that is not annealed; (c) Nyquist diagram of annealed buckypaper; (d) CV diagram of annealed buckypaper.

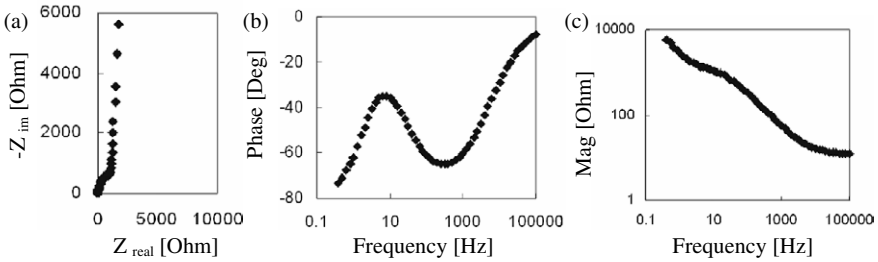


**Figure 2.** Dynamic EIS impedance test of 10% (wt) SWNT/PMMA composite sample in 3% NaCl electrolyte: (a) Nyquist diagram; (b) Bode diagram (phase); (c) Bode diagram (magnitude).

**Table 1.** Estimated values of parameters of the samples based on the EIS test.

| Sample | $R_p$ ($\Omega$) | $C_d$ ($\mu$F) | $W$ ($\mu$S) |
|---|---|---|---|
| (Not annealed) buckypaper | 300.0 | 1.2 | — |
| (Annealed) buckypaper | 24.9 | 3.2 | — |
| SWNT/PMMA 10% composite | 1.15 K | 3.5 | 175.3 |

To verify the electrical modeling of the circuit, a Nyquist plot was simulated based on the estimated parameters. If we assume that the electrical model of the SWNT sensor is as shown in figure 3(a), the impedance of the circuit can be found using the following equations. The impedance of a capacitor ($z_C$) in the time domain is:

$$z_C(t) = \frac{v(t)}{i(t)} = \frac{1/c \int i\,dt}{i(t)}. \tag{1}$$

For the frequency domain analysis, if we convert equation (1) to the $S$ domain by using a Laplace transform, the impedance of a capacitor ($Z_C$) is:

$$Z_C(S) = \frac{1}{C_d \cdot S}. \tag{2}$$

The impedance of a resistor ($Z_R$) is:

$$Z_R(S) = R_p. \tag{3}$$

The total impedance of the combination circuit is found by adding reciprocals:

$$\frac{1}{Z(S)} = \frac{1}{Z_R(S)} + \frac{1}{Z_C(S)} = \frac{1 + C_d \cdot R_p \cdot S}{R_p}. \tag{4}$$

The impedance in the frequency domain becomes:

$$Z(j\omega) = Z_{re} + jZ_{im} = \frac{R_p}{1 + (\omega C_d R_p)^2} - j\frac{\omega C_d R_p^2}{1 + (\omega C_d R_p)^2}. \tag{5}$$

A Nyquist plot is made using equation (5) and the parameters of buckypaper in table 1. This result is shown in figure 3(c) and it is identical with the curve fit in figure 1(c).

An electrical model of the nanocomposite is required in order to optimize its sensing characteristics in electrical circuits. It is also important to know how the sensor impedance parameters are related to the material process. The resistance dominates the strain sensitivity to cracking and it also reduces the sensitivity of long sensors because the resistance becomes too large. The EIS can help us to understand how to improve

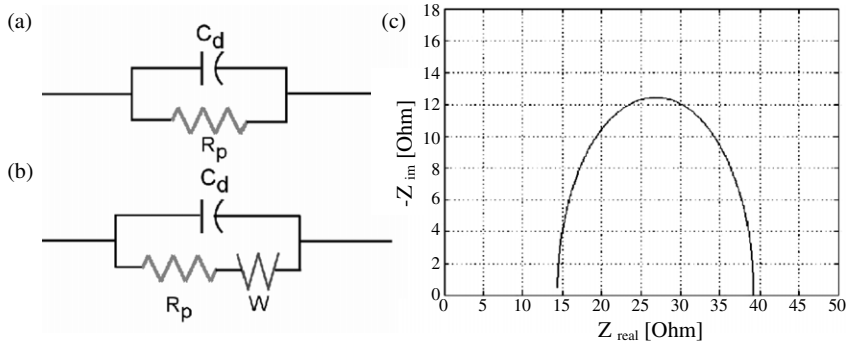


**Figure 3.** Equivalent electrical model and Nyquist diagram: (a) buckypaper; (b) 10% (wt) SWNT/PMMA composite; and (c) simulated Nyquist diagram of buckypaper.

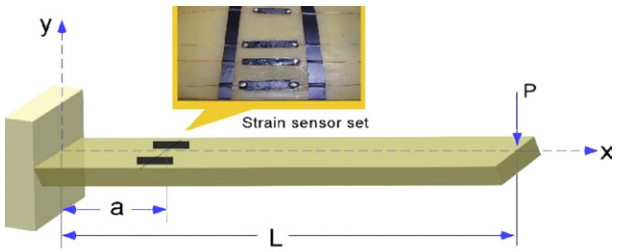


**Figure 4.** A cantilever beam with a strain sensor set.

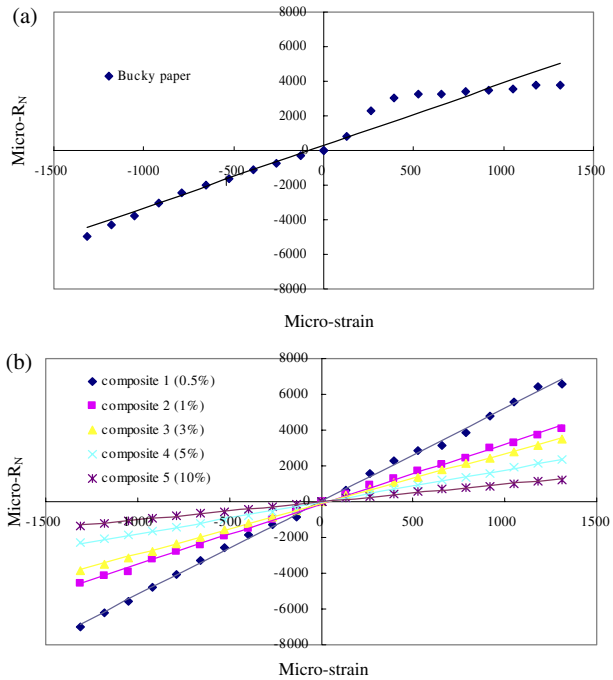


**Figure 5.** Strain modeling of: (a) a buckypaper sensor; (b) SWNT/PMMA composite sensors with different weight percentages of SWNT in the PMMA.

dispersion of the nanotube in the polymer to reduce the resistance, and this will help to design a longer continuous strain sensor. It is expected that improved sensitivity and longer sensors can be obtained from the improved composite fabrication process.

## 3. Strain response modeling and sensitivity of the sensor on a dry structure

A set of CNT strain sensors was attached to the surface of a fiberglass beam. A fiberglass cantilever beam was used because it is a simple structure for modeling and testing the response of the sensor. One end of the beam was clamped to a table as shown in figure 4. Each strain sensor was tightly bonded using a vacuum bonding method to ensure that the superglue makes a stiff bond to transfer the strain across the sensor without any slippage. The sensors were connected to wires with silver conducting epoxy to reduce the contact resistance. The beam end displacements and change of resistance of the individual sensors on the beam were measured when the beam was deflected.

It has been reported that the electrical properties of SWNTs show a change over a wide temperature range [45, 46], and change due to pressure [47] and also due to certain chemical environments [48, 49]. Since we are developing a resistance strain sensor, it is assumed that the resistance of the SWNT based sensor only changes due to strain, and the capacitance does not change in this study. The change of resistance of each strain sensor was measured with respect to the displacement due to bending of the cantilever beam. The strain in the beam ($\varepsilon$) was derived from cantilever beam theory [50] as shown next. Using beam theory, the stress in the beam is:

$$\sigma = \frac{Mc}{I} \tag{6}$$

where $M$, $I$ are the internal bending moment in the beam and the bending inertia of the beam, respectively, $c = t/2$ is the distance from the neutral axis to the surface of the beam where the strain sensor is bonded and $t$ is the thickness of the beam. For a rectangular beam $I = bt^3/12$, where $b$ is the width of the beam. For the case of a cantilever beam with a load at the free end, the internal moment, $M$, in the beam at the strain sensor is

$$M = P(L - a) \tag{7}$$

where $P$ is the load, $a$ is the distance from the fixed end of the beam to the center of the location of the strain sensor and $L$ is

**Table 2.** Measured beam parameters.

| Beam length | Beam thickness | Beam width | Fixed end to center of sensor | Sensor dimension |
|---|---|---|---|---|
| $L = 380$ mm | $t = 4$ mm | $b = 75$ mm | $a = 140$ mm | $5 \times 30 \times 0.3$ mm$^3$ |

the length of the beam. Solving for the strain in the beam using (6) and (7) gives:

$$\varepsilon = \frac{\sigma}{E} = \frac{P(L-a)c}{IE} \tag{8}$$

where $E$ is the elastic modulus of the beam. If a perfect bond is assumed between the beam and the strain sensor, then the strain at the surface of the beam and the strain in the sensor will be identical. In the experiments performed, the beam will be displaced by a known amount at the free end. Beam theory is used to determine the load in terms of the displacement at the end. The load can be substituted into (8) to obtain the strain at the location of the sensor due to the displacement of the free end of the beam. The displacement at the free end of the beam $y(L)$ due to the concentrated force at the end ($P$) is:

$$y(L) = \frac{PL^3}{3EI}; \tag{9a}$$

or

$$P = \frac{3EI}{L^3} y(L). \tag{9b}$$

Then substituting equation (9*b*) into equation (8) gives the strain at the strain sensor:

$$\varepsilon = \frac{3c(L-a)}{L^3} y(L). \tag{10}$$

Equation (10) will be used to convert beam displacement to strain in the modeling. The change in resistance of the strain sensors was measured with a multi-meter and the values were converted to a normalized change of resistance ($R_N$):

$$R_N = \frac{R_s - R_0}{R_0} \tag{11}$$

where $R_0$ is the resistance without any displacement or strain and $R_s$ is the measured sensor resistance when the beam is strained. Table 2 shows the estimated beam parameters used to find the strain. Figure 5 shows the change of resistance of the strain sensors with respect to the change of strain.

In this experiment, the slope of the curve represents the sensitivity of each strain sensor. The data shown are the average values of five strain measurements for each sample. The test was conducted only in the elastic displacement range. In the future, the linearity test will be performed above the elastic structural deformation range to test the ability of the composite sensor to measure large strain. The strain response of buckypaper shows a higher sensitivity than other composite sensors in the linear bending range, but in tension it shows a saturated nonlinear behavior above the 500 microstrain range. This is probably due to the contact separation and slip of the SWNTs which are entangled with simple mechanical bonding in the buckypaper. In beam compression, the buckypaper sensor does not show saturation in the strain response. There is probably less slip of individual SWNTs during compression. Even though the buckypaper shows piecewise linearity, the buckypaper may not be suitable for measuring strain in the whole elastic range. While the composite strain sensors show less sensitivity than buckypaper, they show quite a linear symmetric strain response in both compressive and tensile bending cases. Because the polymer bonding prevents sensor slippage, it effectively improves the strain transfer across the composite sensor and shows a linear strain response with load. The sensitivity of the strain sensor is defined as the gage factor ($S_g$) which relates the change in resistance to the axial strain ($\varepsilon_a$) [51]. From the definition of gage factor, the gage factors of each sensor can be found using equation (12) and they are the slopes of the curves in figure 5:

$$S_g = \frac{\Delta R_N}{\Delta \varepsilon}. \tag{12}$$

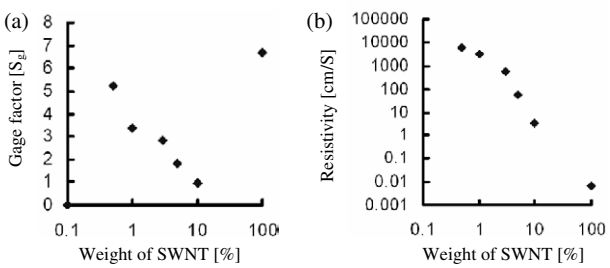


**Figure 6.** Gage factor (a), and resistivity (b), of SWNT buckypaper and PMMA based strain sensors.

Figure 6(a) shows the gage factors for the SWNT buckypaper and SWNT/PMMA sensors. The gage factor of buckypaper formed using 100% SWNT is higher than the other composite samples in the small strain range. Figure 6(b) shows the resistivity of the samples which is computed based on the resistance and dimensions of the samples. The lower percentage of SWNT in the composite sensor shows a higher sensitivity, except for buckypaper. This study shows the freedom to design the gage factor or resistance by controlling the ratio of polymer to SWNTs under optimized dispersion processing. The optimized sensitivity considering the weight of SWNTs is achieved in the 3–10% SWNT mixing range. The percolation threshold of the composite was 0.1% which is little higher than in Kim's study [52] (which was 0.074%), and also the conductivity range seems to be quite reasonable in the present study.

## 4. Dynamic strain test of the sensor on a beam

The experimental setup to test the dynamic response of the SWNT based strain sensors is shown in figure 7. All experiments were done at room temperature. The 10% SWNT/PMMA composite sensor was selected for the experiment. Since the other SWNT/PMMA composite strain sensors have higher resistance, they require a higher driving

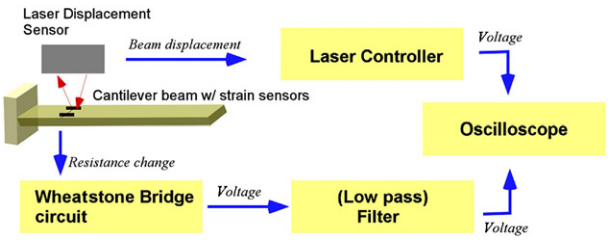


**Figure 7.** Test setup of the SWNT based strain sensor to measure dynamic strain.

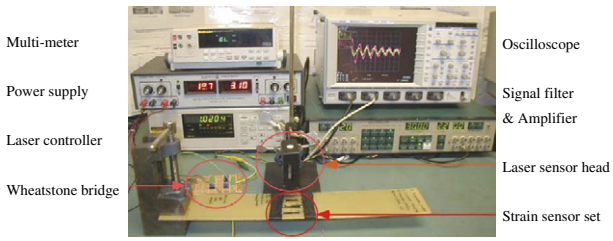


**Figure 8.** Photograph of the experimental setup.

voltage and need more current. The higher resistance also causes broad band noise because of the low current flow in the circuit. This makes signal processing more difficult and a filter and amplifier are needed with a 20 V applied voltage. As CNTs can be either metallic or semiconducting, depending on the chirality of the tube, the buckypaper simultaneously has metallic (high conductivity) and semiconducting properties [53]. The SWNT based sensors show resistance drift due to ambient temperature and other effects similar to conventional metallic strain gages. Thus, a dummy SWNT strain gage is connected to the Wheatstone bridge to compensate for the resistance drift. The drift and its compensation are still being investigated to reduce sensor error.

The instrumentation and entire experimental setup are shown in figure 8. A laser displacement sensor (Keyence, LC-2400 series) is used to measure the displacement of the strain sensor. The laser sensor measures beam displacement at the center of the strain sensor and the measurement is used to find the actual strain in the beam at this point; this is compared to the simulation result described next.

The buckypaper strain sensor was tested using a 5 V driving voltage for the Wheatstone bridge. The signal was measured with a 30 Hz low-pass filter with a 20 dB amplification gain. Figure 9 shows the dynamic strain response of the sensors in free vibration induced by displacing and releasing the free end of the beam. Above 500 microstrain, the dynamic strain response of the buckypaper showed a decreasing sensitivity due to slip of the SWNTs as described earlier. The buckypaper sensor does not exactly represent beam displacement, as shown by comparison with the laser displacement sensor in figure 9(a). The SWNT/PMMA 10% composite sensor was tested with a 20 V driving voltage with a 30 Hz cutoff low pass filter with a 20 dB gain. The sensor response in figure 9(b) is almost identical with the output of the laser displacement sensor, which means that the composite sensor measures the strain signal from the structure without much distortion.

## 5. Electrical modeling and simulation of the dynamic strain response

An electrical model of the voltage response from the strain sensor using the Wheatstone bridge was derived. The electrically parallel circuit model of the sensor was based on the EIS test model with electrolyte as shown in figure 3. The composite has a diffusion parameter and Warburg coefficient in the model but they were neglected in the simple electrical model in equation (5) for dry structural applications in this study. The dry sensor in particular has much smaller capacitance than the wet sensor, but the same electrical model is used.

The change of resistance can be converted into a Wheatstone bridge voltage output ($V_{out}$) with a DC power source ($V_{drv}$); the voltage output should be:

$$V_{out} = \pm(V_{11} - V_{21}) \tag{13}$$

where $V_{11}$ and $V_{21}$ are the voltage across the strain sensor and the resistance $R_2$, respectively. The circuit driving voltage ($V_{drv}$) coming from the external power supply can be expressed as the sum of $V_{21}$ and $V_{22}$, which is the voltage across resistance $R_3$:

$$V_{drv} = V_{21} + V_{22}. \tag{14}$$

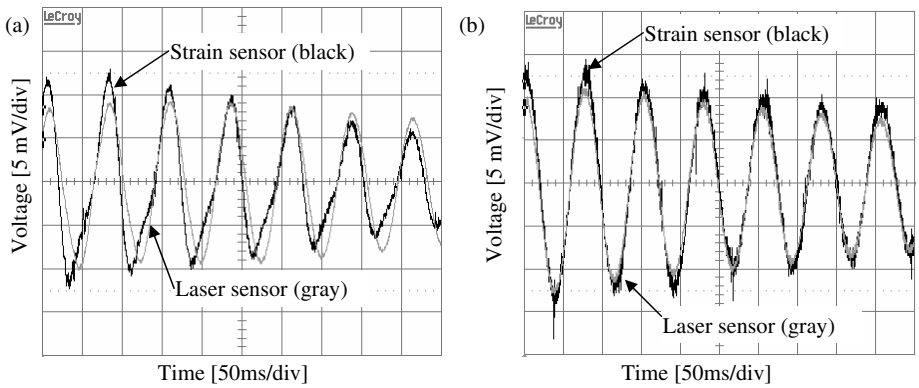


**Figure 9.** Dynamic strain response in a free vibration beam (cutoff frequency 30 Hz, gain 20 dB): (a) response of the buckypaper strain sensor; (b) response of the SWNT/PMMA 10% strain sensor.

**Table 3.** Simulation parameters.

| | | | | |
|---|---|---|---|---|
| Sensor resistance | Sensor capacitance | Gage factor | Bridge resistance | |
| $R_s = 2.41$ kΩ | $C_s = 245$ pF | $S_g = 1.76$ | $R_1 = R_2 = R_3 = 2.41$ kΩ | |
| Fixed end to center | Max. $y$ displacement | Beam freq. | Amp. gain | Driving voltage |
| of sensor $a = 163$ mm | of sensor $y(a) = 1$ mm | $f = 12.5$ Hz | 20 dB | $V_{drv} = 20$ V |

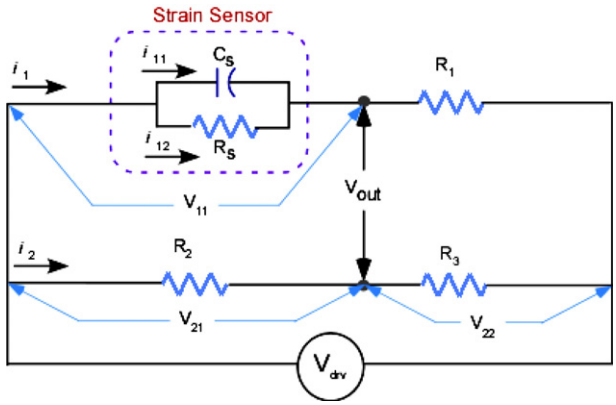


**Figure 10.** Electrical circuit model of the composite strain sensor and Wheatstone bridge.

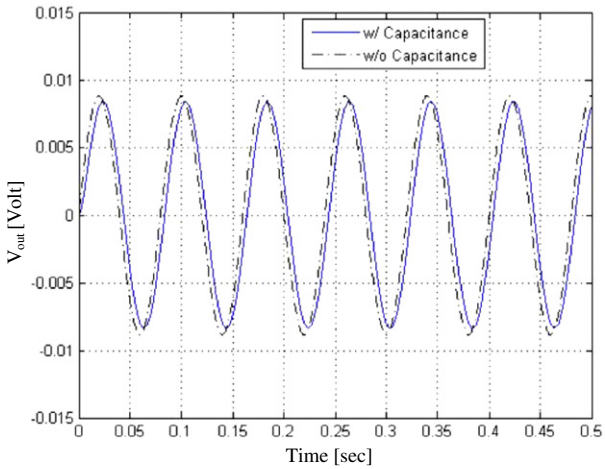


**Figure 11.** Simulation of the strain response of the SWNT/PMMA 10% sensor on a cantilever beam.

Solving for the voltage ($V_{21}$) with Ohm's law:

$$V_{21} = R_2 i_2 = \frac{R_2}{R_2 + R_3} V_{drv}. \tag{15}$$

Solving for the voltage ($V_{11}$):

$$V_{11} = V_{drv} - R_1 i_1. \tag{16}$$

Applying Kirchoff's first law [54] to find the current flowing the strain sensor ($i_1$) gives

$$i_1 = i_{11} + i_{12} = C_s \dot{V}_{11} + \frac{V_{11}}{R_c} \tag{17}$$

where $C_s$ and $R_s$ are the capacitance and resistance, respectively, of the strain sensor. In this study, only $R_s$ is a variable with respect to dynamic strain while $C_s$ is assumed a constant independent of the change of strain. Substituting equation (17) into (16) produces a non-homogenous first order, ordinary, but non-linear differential equation which describes the voltage across the strain sensor:

$$R_1 C_c \dot{V}_{11} + (1 + R_1/R_s(\varepsilon))\, V_{11} = V_{drv}. \tag{18}$$

In (18), the resistance of the strain sensor ($R_s$) and the voltage across it ($V_{11}$) change simultaneously because dynamic strain simultaneously changes the resistance of the strain sensor and the voltage across it. Therefore, in order to find $V_{11}$, it is first necessary to find $R_c$ using the strain model which can be found from the gage factor and the strain of the beam, and this procedure is shown below. After that, the solution of $V_{11}$ is found using numerical integration. The voltage output in equation (13) can be obtained from the solution of equations (18) and (15).

The response of the strain sensor was simulated by solving equation (18). The resistance corresponding to a 10% SWNT/PMMA composite sensor was selected for the simulation, and to verify the sensor modeling. The resistance change in the strain sensor $R_s$ is

$$R_s(\varepsilon) = R_0 + \Delta R \tag{19}$$

where $R_0$ is original resistance of the strain sensor without any strain and $\Delta R$ is the change of resistance due to beam deflection, which can be deduced from the previous strain modeling curve (figure 5). The previous modeling was measured during a continuous change of displacement, but for the dynamic change of displacement the strain response shows a smaller change of resistance. This might be due to hysteresis of the sensor, and is still being investigated. Thus, the gain factor ($S_g$) is measured again for the dynamic strain simulation for the SWNT/PMMA wt 10% composite sensor. The change in resistance due to dynamic strain can be found using (12) and is

$$\Delta R = R_0 \times S_g \times \varepsilon. \tag{20}$$

The dynamic strain of the beam was derived from the measurement of the $y$ displacement of the center of the sensor, $y(a)$, measured with the laser displacement sensor in figure 10(b). The beam frequency ($f$) was also determined based on the time response in figure 9(b). Table 3 gives the simulation parameters. As this is a study for a dry structural application, the resistance and capacitance of the sensor were measured with a multi-meter and a capacitance meter, respectively.

Finally, the voltage output from the Wheatstone bridge was found from equation (13) and by solving equation (18) using the Runge–Kutta fourth order method [55]. Figure 11 shows the simulation of the strain response of the SWNT/PMMA composite sensor. The simulation assumed

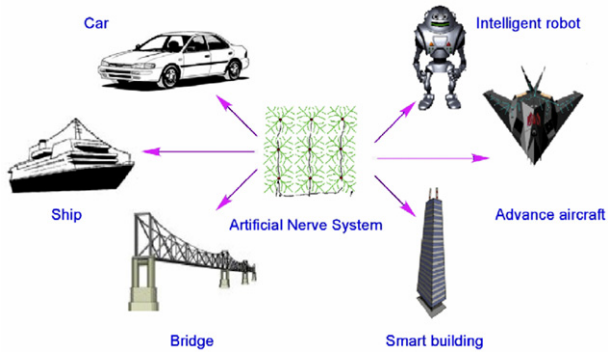


**Figure 12.** A CNT based artificial neural system and its applications.

undamped vibration in the beam, therefore the strain response does not show the decay of vibration amplitude which is shown in the experiment. If there is no initial strain, the voltage across the sensor ($V_{11}$) is the same as the voltage across resistance $R_1$($V_{12}$) and the initial condition of equation (18), the initial voltage across the sensor, can be assumed to be half of $V_{\mathrm{drv}}$. This simulation shows good agreement with the strain response of the actual sensor. The amplitude of the simulated voltage output is 13% smaller than the actual sensor output, probably due to modeling error. Most of the error may come from the non-linear characteristics of the sensor, especially the resistance drift. Hence, drift modeling or a compensation method should be studied to improve the simulation.

The effect of the capacitance term parallel to the resistance in the electrical model is also considered. The solid line in figure 11 shows the strain response of the sensor with the capacitance term in the model of the resistance strain gage. The parallel capacitance combination causes a small phase delay of the signal [56], and it reduces the voltage amplitude because of the drop in current due to the capacitance. In most the cases, the SWNT based strain sensor can be modeled using only a resistance term because of the small effect of the capacitance term.

## 6. An artificial neuron based on a MWNT strain sensor

CNTs can be fabricated as long films [57–59], which can be considered as a long continuous neuron sensor. The neurons can be connected in parallel with logic circuits to form a neural system. The neural system can be in the form of a grid attached to the surface of a structure to make a sensor network, like the neural system in the human body. This would be an artificial neural system (ANS) for SHM and would cover large areas and monitor a structure in real time [60, 61]. The architecture for a neural system has already been developed for piezoelectric neurons. Nanotube neurons would be a simpler type of neuron and could be integrated into an existing structural neural system [70]. Figure 12 shows the concept of a biomimetic ANS which could be built with CNT continuous strain sensors.

The CNT neurons used to form an artificial neural system can detect large strains in a structure at distributed points. A CNT based ANS may therefore have applications such as in a smart crash detection system in automobiles [62] and structural health monitoring of metallic and composite structures. The ANS not only senses the strain of the structure but also predicts the location of cracks within a grid of sensors [63]. By controlling the stiffness of the neuron with different strengths of the binding polymer, we can also build soft or hard neurons. For instance, a hard neuron is suitable for structural strain measurement and a soft neuron may be suitable for artificial skin because it can simultaneously sense large strains, pressure and temperature. The flexibility of soft neurons may allow them to be embedded in artificial skin with a tactile sense for an intelligent robot. A crack propagating near the neuron may increase the strain of the sensor, and if the crack reaches the sensor it will reduce the area or completely separate the neuron. Because the neuron is made of long, thin CNTs it can be easily separated by a small crack and it can be highly distributed across the structure; therefore it could sense and prevent catastrophic damage, for example in aircraft and launch vehicles.

Large scale structures such as bridges and buildings need to directly measure the long-span and multi-dimensional strain occurring these structures. However, it is difficult to install a sufficient number of conventional strain gages as they require a large amount of wiring [64]. An ANS is made from long continuous CNT sensors and can monitor continuous strain along a bridge or building. Furthermore, this type of neuron is a resistance type of electrical strain sensor and can become an industrially viable technique by just using a simple bridge circuit. The neuron could be highly distributed across the structure and could sense and prevent catastrophic damage. An ANS formed using CNT neurons could monitor strain over long sections of a structure as an alternative to the piezoelectric ceramic neurons used in the SNS described in [65, 70]. CNT neurons are lighter than the piezoelectric system. Furthermore, such a neuron could cover a larger area than a localized strain gage, and a nanotube neuron is easier to install or embed into a structure because the ANS sensor system can be sprayed on with an airbrush using a template to outline the neurons. The neurons could also be inserted into the structure as a pre-cured layered film. CNT neurons would add almost no penalty to the structure because a CNT ANS is lightweight and thin, there is no stress concentration, no piezoelectrics and no storage of high frequency waveforms which is required in some other SHM methods. Such an ANS is expected to effectively detect damage in large complex structures including composite helicopter blades and composite aircraft and rotorcraft.

The cost of nanotube neurons may be high for use on large structures with long SWNT neurons. Building an ANS with MWNTs or multi-walled carbon nanofiber (CNF) instead of SWNTs would reduce the cost in real applications. A MWNT has lower performance but is about one-quarter of the cost of SWNTs. A CNF has lower performance again, but is about 200 times lower in cost than a SWNT sensor. Although SWNTs have excellent electrochemical properties, because their cost is high and incorporation of SWNTs into polymers at high loadings is difficult, MWNT and CNF composite continuous strain sensors are being developed further in our laboratory. CNFs are similar to large diameter MWNTs, but the nanofibers are not continuous tubes and their surfaces show steps at the termination of each tube wall[4].

[4] Applied Sciences Inc., and Pyrograf Products, Inc., contact person, Mr David Burton.

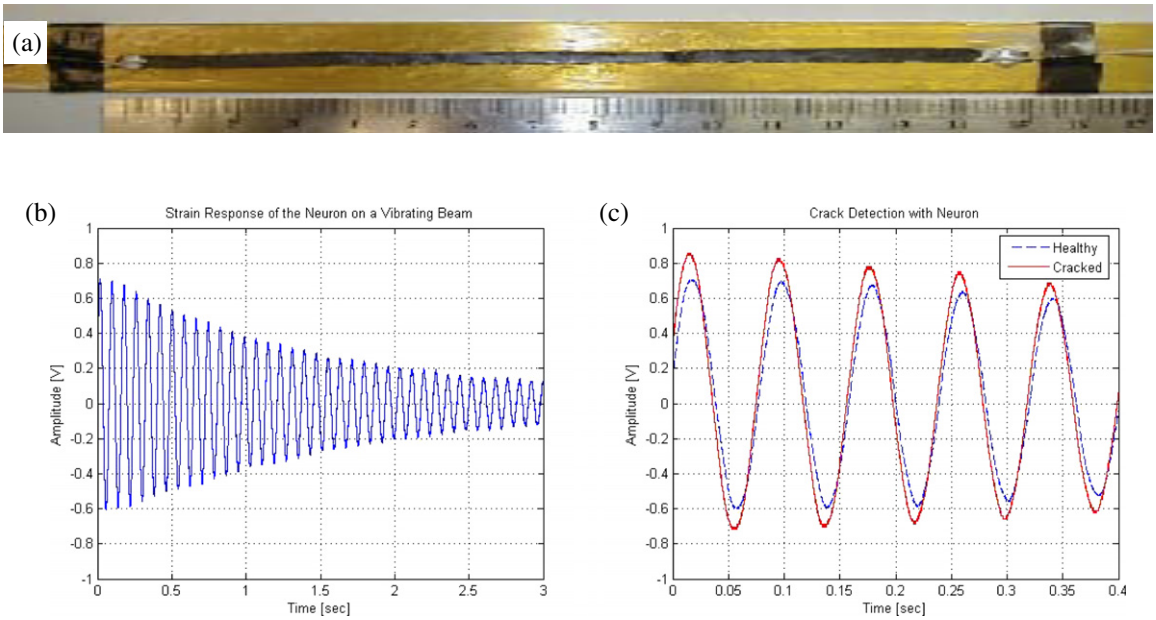


**Figure 13.** A MWNT neuron continuous strain sensor and its dynamic strain response after low-pass filtering (cutoff frequency 30 Hz, 60 dB gain): (a) MWNT/PMMA wt.10% neuron (150 mm × 4 mm × 0.08 mm, 3.7 kΩ) on a fiberglass plate; (b) dynamic strain response on a vibrating beam; (c) voltage and phase change due to crack propagation on the neuron on a vibrating beam.

Figure 13 shows a MWNT/PMMA wt.10% composite neuron and its strain response in an aluminum cantilever. The composite neuron is patterned on the structure using a spray-on technique. This makes it easy to apply the neuron to existing structures for SHM applications. The spray strain sensor could be used not only in large structures but also on microstructures such as MEMS. Having smaller mechanical and electrical properties than SWNTs, a MWNT neuron shows less strain sensitivity but the MWNT/PMMA neuron shows fairly high sensitivity to the change in strain on a cantilever with appropriate signal processing. Figure 13(a) shows a neuron installed on an aluminum beam with a yellow Kapton insulating layer. Figure 13(b) shows the dynamic strain response of the neuron. The response matches well with the vibration measured using a laser displacement sensor. The neuron is a thin layer of composite material and it will be separated when a crack propagates through it. After the separation, the resistance of the sensor is increased and the capacitance is decreased, which can be converted into a voltage response change using a bridge electrical circuit. The reduced resistance due to damage causes a higher amplitude voltage and the reduced capacitance induces a phase shift of the dynamic response. Figure 13(c) shows the response from an experiment to simulate crack detection on an aluminum beam with a MWNT/PMMA neuron. The neuron is partly cut with a blade to simulate propagation of a crack through the neuron. A thin cut to simulate a crack is used to avoid the long fatigue testing of the beam needed to generate a crack. The simulated crack gives a similar result to the actual fatigue cracking that was performed on earlier samples. The 2 mm crack through half the width of the neuron produced a simultaneous change of resistance and capacitance. The resistance and capacitance of the neuron were changed from 3.7 to 3.8 kΩ and from 31.1 to 29.0 pF, respectively. Since the neuron has resistance and capacitance terms as sensing parameters, and the neuron is small and lightweight, SHM using the neuron will be more practical than using other larger more expensive sensor types. Conventional crack detection techniques are based on local stress detection due to a stress concentration [66] or measuring only the change of resistance due to cutting a foil crack sensor as a result of crack propagation [67]. However, the neuron determines crack propagation based on two electrical parameters that can simultaneously monitor different SHM parameters at the same location [68]. Each neuron of the ANS can monitor the average strain along it by a change of resistance and simultaneously monitor a change of capacitance if a crack breaks the neuron. The CNT neuron is smaller and simpler then other sensor types for building an ANS. After completely separating the neuron, the AC voltage output from the circuit goes to zero due to the open circuit. The strain sensing model and its structural damage detection characteristics for SHM are being further investigated, including the use fatigue testing. The effect of the width and thickness of the neuron on the sensitivity to damage are also being investigated.

## 7. Conclusions

Having tailored mechanical properties and piezoresistive properties, a SWNT based resistance sensor was able to measure the strain in structures. Experimentation showed that a buckypaper strain sensor has high sensitivity, but because of the weak axial van der Waals attraction nanotube slippage degrades the strain response of the sensor which was linear only within the range of 500 microstrain. The buckypaper strain sensor could not exactly represent the beam strain in a dynamic load test. Therefore, a CNT/PMMA composite sensor was developed to improve the strain transfer across the

sensor by means of stronger polymer interfacial bonding. Even though the composite strain sensor showed a lower sensitivity than the buckypaper sensor, it has a fairly linear symmetric strain response under static and dynamic strain.

An electrical model of the nanotube sensor was derived based on electrochemical impedance spectroscopy and static resistance tests. The sensor was also modeled, and the dynamic response of the sensor on a beam was simulated. The simulation showed good agreement with the strain response of the actual sensor. The capacitance effect of the sensor was considered and found to have a small effect on the dynamic response.

Finally, a biomimetic artificial neuron was developed using a MWNT composite continuous strain sensor. The neuron is a low cost sensor suitable for SHM of large structures. Since this long sensor is easy to apply to a structure using a spray-on technique, it could be utilized to build an artificial neural system. In addition, this neuron is a resistance type electrical strain sensor and it can be used with simple circuitry like a conventional strain gage. The neuron is able to detect a small crack propagating through it under dynamic loading. The crack induces a change in the voltage amplitude and phase during vibration.

Further study of the large strain sensing capability of the nanotube sensor is aimed at increasing the bandwidth of the dynamic response, minimization or correction of resistance drift and determination of the long term reliability of the sensor material. This will prepare CNT based sensors for practical applications.

## References


[1] Iijima S 1991 Helical microtubules of graphitic carbon *Nature* **354** 56–8

[2] Ajayan P M and Zhou O 2001 Applications of carbon nanotubes *Carbon Nanotubes Synthesis, Structure, Properties and Applications* ed M S Dresselhaus, G Dresselhausand and Ph Avouris (Berlin: Springer)

[3] Baughman R H, Sakhidov A A and de Heer W A 2002 Carbon nanotubes—the route toward applicatins *Science* **297** 787–92

[4] Peng S, O'Keeffe J, Wei C, Cho K, Kong J and Chen R 2003 Carbon nanotube chemical and mechanical sensors *3rd Int. Workshop on Structural Health Monitoring (15–17 September 2003, Stanford, CA)*

[5] Ghosh S, Sood A K and Kumar N 2003 Carbon nanotube flow sensors *Science* **299** 1042–4

[6] Wood J R and Wagner H D 2000 Single-wall carbon nanotubes as molecular pressure sensors *Appl. Phys. Lett.* **76** 2883–5

[7] Kong J, Frankin N R, Zhou C, Chapline M G, Peng S, Cho K and Dai H 2000 Nanotube molecular wires as chemical sensors *Science* **287** 622–5

[8] Baughman R H *et al* 1999 Carbon nanotube actuators *Science* **284** 1340–4

[9] Tahhan M, Truong V-T, Spinks G M and Wallace G G 2003 Carbon nanotube and polyaniline composite actuators *Smart Mater. Struct.* **12** 626–32

[10] Smela E 2003 Conjugated polymer actuators for biomedical applications *Adv. Mater.* **6** 481–94

[11] Peng S and Cho K 2000 Chemical control of nanotube electronics *Nanotechnology* **11** 57–60

[12] Wood J R, Zhao Q, Frogley M D, Neurs E R, Prins A D, Peijs T, Dunstan D J and Wagner H D 2000 Carbon nanotubes: from molecular to macroscopic sensors *Phys. Rev.* B **62** 7571–5

[13] Dharp P, Li Z, Nagarajaiah S and Barrera E V 2004 Nanotube film based on single-wall carbon nanotubes for strain sensing *Nanotechnology* **15** 379–82

[14] Zhao Q, Frogley M D and Wagner H D 2002 Direction-sensitive strain-mapping with carbon nanotube sensors *Compos. Sci. Technol.* **62** 147–50

[15] Park J, Kim D, Lee J and Kim T 2003 Nondestructive damage sensing and reinforcing effect of carbon fiber/epoxy-carbon nanotube or nanofiber composites using electro-micromechanical techniques *ICCE-10 Conf.* pp 551–2

[16] Watkins A N, Ingram J L, Jordan J D, Wincheski R A, Smits J M and Williams P A 2004 Single wall carbon nanotube-based structural health monitoring sensing materials *NSTI Conf.—Nanotech 2004* vol 3, p 149

[17] Hilding J, Grulke E A, Zhang Z G and Lockwood F 2003 Dispersion of carbon nanotubes in liquids *J. Dispersion Sci. Technol.* **23** 1–41

[18] Moore V C, Strano M S, Haroz e H, Hauge R H and Smalley R E 2003 Individually suspended single-walled carbon nanotubes in various surfactants *Nano Lett.* **3** 1379–82

[19] Zhu J, Kim J, Margrave J L, Khabashesku V N and Barrera E V 2003 Improving the dispersion and integration of single-walled carbon nanotubes in epoxy composites through functionalization *Nano Lett.* **3** 1107–13

[20] Lu K L *et al* 1996 Mechanical damage of carbon nanotubes by ultrasound *Carbon* **34** 814

[21] Sslam M F, Rojas E, Bergey D M, Johson A T and Yodh A G 2003 High weight fracton surfactant solubilization of sing-wall carbon nanotubes in water *Nano Lett.* **3** 269–73

[22] Liu J *et al* 1998 Fullerene pipes *Science* **280** 1253–6

[23] Carbon Nanotechnologies Incorporated http://www.cnanotech.com/

[24] Ajayan P M, Ravikumar V and Charlier J-C 1998 Surface reconstructions and dimensional changes in single-walled carbon nanotubes *Phys. Rev. Lett.* **81** 1437–40

[25] Rinzler A G *et al* 1998 *Apply. Phys.* A **67** 29–37

[26] An K, Kim W, Park Y, Choi Y, Lee S, Chung D, Bae D, Lim S and Lee Y 2001 Supercapacitors using single-walled carbon nanotube electrodes *Adv. Mater.* **13** 497–500

[27] An K H, Kim W S, Park Y S, Moon J, Bae D J, Lim S C, Lee Y S and Lee Y H 2001 Electrochemical properties of high-power supercapacitors using single-walled carbon nanotube electrodes *Adv. Funct. Mater.* **11** 387–92

[28] Lordy V and Yao N 2000 Morecular mechanics of binding in carbon-nanotube-polymer composites *J. Mater. Res.* **15** 2770–9

[29] Liao K and Li S 2001 Interfacial characteristics of a carbon nanotube-polystyrene composite system *Appl. Phys. Lett.* **79** 4225–7

[30] Penumadu D, Dutta A, Pharr G M and Files B 2003 Mechanical properties of blended single-wall carbon nanotube composites *J. Mater. Res.* **18** 1849–53

[31] Xu X and Thwe M M 2002 Mechanical properties and interfacial characteristics of carbon-nanotube-reinforced epoxy thin films *Appl. Phys. Lett.* **81** 2833–5

[32] Wong M, Paramsothy M, Xu X J, Ren Y, Li L and Liao K 2003 Physical interactions at carbon nanotube-polymer interface *Polymer* **44** 7757–64

[33] Coleman J N, Blau W J, Dalton A B, Munzo E, Collins S, Kim B G, Razal J, Selvidge M, Vieiro G and Baughman R H 2003 Improving the mechanical prpperties of single-walled carbon nanotube sheets by intercalation of polymeric adhesives *Appl. Phys. Lett.* **82** 1682–4

[34] Yang Z and Wu H 2001 The electrochemical impedance measurements of carbon nanotubes *Chem. Phys. Lett.* **343** 235–40

[35] Niu C, Sichel E K, Hoch R, Moy D and Tennent H 1997 High power electrochemical capacitors based carbon nanotube electrodes *Appl. Phys. Lett.* **70** 1480–2

[36] http://www.gamry.com/App_Notes/EIS_Primer/EIS_Primer.htm
[37] Park S M and Yoo J S 2003 Electrochemcial impedance spectroscopy for better electrochemical measurements *Anal. Chem.* **75** 455–61
[38] http://www-biol.paisley.ac.uk/marco/Enzyme_Electrode/Chapter1/Cyclic_Voltammetry1.htm
[39] Prokudina N A, Shishchenko E R, Joo O S, Kim D Y and Han S H 2000 Carbon nanotube RLC circuits *Adv. Mater.* **12** 1444–7
[40] Zhao Y P, Wei B Q, Ajay P M, Ramanath G, Lu T M, Wang G C, Rubio R and Roche S 2001 Frequecy-dependent electrical transport in carbon nanotubes *Phys. Rev.* B **64** 201402(R)
[41] Burke P J 2002 Luttinger liquid theory as a model of the gigahertz electrical properties of carbon nanotubes *IEEE Trans. Nanotechnol.* **1** 129–44
[42] Burke P J 2003 An RF circuit model for carbon nanotubes *IEEE Trans. Nanotechnol.* **2** 55–8
[43] Burke P J 2003 Carbon nanotube devices for GHz to THz applications *Proc. 2003 Int. Semiconductor Device Research Symp.*
[44] Valentini L, Puglia D, Frulloni E, Armentano I, Kenny J M and Santucci S 2004 Dielectric behavior of epoxy matrix/single-walled carbon nanotube composites *Compos. Sci. Technol.* **64** 23–33
[45] Kane C L *et al* 1998 Temperature-dependent resistivity of single-wall carbon nanotubes *Europhys. Lett.* **41** 683–8
[46] Bezryadin A, Verschueren A R M, Tans S J and Dekker C 1998 Multiprobe transport experiments on individual single-wall carbon nanotubes *Phys. Rev. Lett.* **80** 4036–9
[47] Bozhko D *et al* 1998 Resistance vs. pressure of single-wall carbon nanotubes *Appl. Phys.* A **67** 75–7
[48] An K H *et al* 2004 Enhanced sensitivity of a gas sensor incorporation singel-walled carbon nanotube-polypyrrole nanocomposites *Adv. Mater.* **16** 1005–9
[49] Collins P G *et al* 2000 Extreme oxygen sensitivity of electronic properties of carbon nanotubes *Science* **287** 1801–4
[50] Beer F P and Johnston E R Jr 1992 *Mechanics of Materials* 2nd edn (New York: McGraw-Hill)
[51] Dally J W and Riley W F 1990 *Experimental Stress Analysis* 3rd edn (New York: McGraw-Hill)
[52] Kim B, Lee J and Yu I 2003 Electrical properties of single-wall carbon nanotube and epoxy composites *J. Appl. Phys.* **94** 6724–8
[53] Dresselhaus M S, Dressehaus G and Eklund P C 1996 *Science of Fullerenes and Carbon Nanotubes* (San Diego, CA: Academic)
[54] Benson H 1991 *University Physics* revised edn (New York: Wiley)
[55] Charpra S C and Canale R P 1989 *Numerical Methods for Engineers* 2nd edn (New York: McGraw-Hill)
[56] Gileadi E 1993 *Electrode Kinetics for Chemists, Chemical Engineers, and Materials Scientists* (New York: VCH)
[57] Ko F, Gogotsi Y, Ali A, Naguib N, Ye H, Yang G, Li C and Willis P 2003 Electrospinning of continuous carbon nanotube-filled nanofiber yarns *Adv. Mater.* **15** 1161–5
[58] Gommans H H, Alldredge J W, Tashiro H, Park J, Magnuson J and Rinzler A G 2000 Fibers of aligned single-walled carbon nanotubes: polarized Raman spectroscopy *J. Appl. Phys.* **88** 2509–14
[59] Vigolo B, Penicaud A, Coulon C, Sauder C, Pailler R, Journet C, Bernier P and Poulin P 2000 Macroscopic fibers and ribbons of oriented carbon nanotubes *Science* **290** 1331–4
[60] Martin W N, Ghoshal A, Sundaresan M J and Schulz M J 2002 Structural heath monitoring using an artificial neural system *Book chapter in Recent Research Developments in Sound and Vibration, Transworld Research Network, Reference number* TRN/SV/UA/S0008
[61] Pammi S, Brown C, Datta S, Kirikera G R and Schulz M J 2002 Building artificial nerves for structures *Proc. IMEC2002 (New Orleans, LA, Nov. 2002)*
[62] Kim A, Smart crash detection using distributed sensors http://structure.stanford.edu/Project/ResearchProjects/ackim/web_profile.pdf
[63] Kirikera G R, Shinde V, Kang I, Schulz M J, Shanov V, Datta S, Hurd D, Westheider B, Sundaresan M and Ghoshal A 2004 Mimicking the biological neural system using electronic logic circuit *SPIE 11th Int. Symp. Smart Structures (San Diego, CA, March 2004)* (Bellingham, WA: SPIE)
[64] Ohno H, Naruse H, Kihara M and Shimada A 2001 Industrial applications of the BOTDR optical fiber strain sensor *Opt. Fiber Technol.* **7** 45–64
[65] Kirikera G R 2003 An artificial neural system for structural health monitoring *MS Thesis* University of Cincinnati
[66] Tikka J, Hedman R and Silijander A 2003 Strain gauge capabilities in crack detection *The 4th Int. Workshop on Structural Health Monitoring (Stanford, CA, Sept. 2003)*
[67] http://www.vishay.com/brands/measurements_group/strain_gages/mm.htm
[68] Kang I, Lee J W, Choi G R, Jung J Y, Hwang S H, Yoon K J and Schulz M J 2005 Structural health monitoring based on electrical impedance of a carbon nanotube neuron *Proc. ANDE2005: the 1st Int. Conf. on Advanced Nondestructive Evaluation (Sept. 2005)*
[69] Watkins A N, Ingram J L, Jordan J D, Wincheski R A, Smits J M and Williams P A 2004 Single wall carbon nanotube-based structural health monitoring sensing materials *NSTI Conf—Nanotech* vol 3, p 149
[70] Kirikera G R, Shinde V, Schulz M J, Ghoshal A, Sundaresan M J, Allemang R J and Lee J W 2006 A structural neural system for real-time health monitoring of composite materials *Struct. Health Monitor. Int. J.* at press